TransformerLess Partial Voltage Architectures for tripling the power of xCell electrochemical systems

Luc DUMAS--LAUSSINOTTE, Thierry MEYNARD, Jeremi REGNIER
LAPLACE CNRS, 2 rue Camichel, 31071 Toulouse, France

ABSTRACT - The concept of partial power converter is promising since it might bring significant cost, weight, volume and loss reduction. However, in most cases partial power converters include a transformer to redirect power from one part of the circuit to another. This transformer adds cost, weight, volume, losses, and cancels most of the gains promised by the partiality concept. In this paper a TransformerLess Partial Voltage Converter capable of supplying a power up to three times the output power of a standard converter is described and analyzed, its main properties are explained, and an example of application is presented.

Keywords—Partial Power Converter, Batteries, TransformerLess

1. INTRODUCTION

Partial Power Processing (PPP) offers a more efficient alternative to conventional power converters. The core concept involves processing only a fraction of the total power, allowing the majority to flow directly to the load. By easing the burden on the converter, component sizes can be minimized, leading to lower energy losses and reduced thermal concerns. This ultimately enhances the overall efficiency of the system. PPP is particularly well-suited for systems composed of series-connected, independent sources such as batteries or photovoltaic panels. The concept was initially introduced in the 1990s within the aerospace sector [1], with a focus on connecting photovoltaic sources to the converter input based on partial power principles. Today, this approach is more commonly applied in Electric Vehicles ([2], [3]) and Battery Energy Storage System ([4], [5], [6]).

According to [7], PPP architectures can be categorized into two main types: Differential Power Converters (DPC) and Partial Power Converters (PPC). The primary function of DPCs is to correct current imbalances among series-connected elements sharing a common voltage bus. As a result, only the differential power is processed rather than the entire power flow. However, in such architecture, an additional converter is required if regulation of the common voltage bus is necessary [8].

PPCs are designed to manage and regulate the power flow, the current, and the voltage between a source and a load [8]. They can be categorized into two groups: isolated and non-isolated converter topologies. In modern designs, PPCs typically incorporate a transformer or coupled inductor within the converter ([2], [4], [6], [9]). However, magnetic components introduce additional losses, weight and volume-factors that counteract the efficiency and compactness benefits sought with this type of converter architecture.

References [10] and [11] present examples of Fractional Power Converter (FPCs), a subtype of PPCs without galvanic isolation, where only a portion of the battery is interfaced with the converter. A key limitation of this approach is that the selected battery fraction mut be carefully sized to accommodate the charging and discharging demands of the remaining cells. Additionally, this topology does not allow for individual cell current regulation. As a result, imbalances can develop over time between the battery cells, ultimately restricting the usable capacity of the entire battery.

Batteries are electrochemical devices that maintain stable terminal voltage. A simplified model includes an electromotive force (EMF), non-linearly related to the state of charge (SOC) and observed as the open-circuit voltage (OCV), and an equivalent series resistor (ESR) that is responsible for an additional voltage drop and charging-discharging. ESR changes with temperature and aging, making accurate model complex. The topology introduced in this paper relies on the fact that terminal voltage remains in a limited interval in all operating conditions over the battery's lifetime. Data shows this voltage remains within [2.7V; 4.2V] (64.2%-100% in per-unit) [12].

Conventional converters, including those presented in [10], [11], typically provide a voltage variation over the full [0; 100%] range. However, this often results in underutilization of approximately two-thirds of the battery's operating range. In this paper, we explore an alternative architecture capable of regulating voltage strictly within the required range. This approach enables the use of semiconductor devices rated for one-third of the full voltage, offering significant advantages in terms of cost reduction, faster switching, lower losses, decreased size, value, and cost of passive components.

2. TOPOLOGY CONSTRUCTION

The root idea of TransformerLess Partial Voltage Converter (TLPCV) is to switch only a fraction of the source voltage, specifically in the range [2/3;1], rather than the highest voltage. This could theoretically be achieved with a circuit made of a Partial Buck converter and a Capacitive divider (Fig. 1-a).

However, standard PVC architectures face stability issues due to naturally stabilizing the capacitive divider without additional components, increasing cost and losses. A proposed workaround is to symmetrize the circuit (Fig. 1-b), where currents in switches connected to the midpoint compensate due

to equal duty cycles and amplitudes. By adding two additional cells (Fig. 1-c), we still observe two nodes carrying ±*D.I* and two carrying ±*I*. However, the intermediate node appears balanced, suggesting that with this construction, adding any number of additional cells will consistently result in only two problematic nodes at each end. Meanwhile, the internal nodes maintain a zero average current and can remain stable. Given that battery packs often consist of several hundred cells, addressing the issue at these four end-nodes could be worthwhile. This is especially relevant considering that, in doing so, all internal commutation cells would then handle three times the nominal current. Such an approach could potentially optimize the overall system performance.

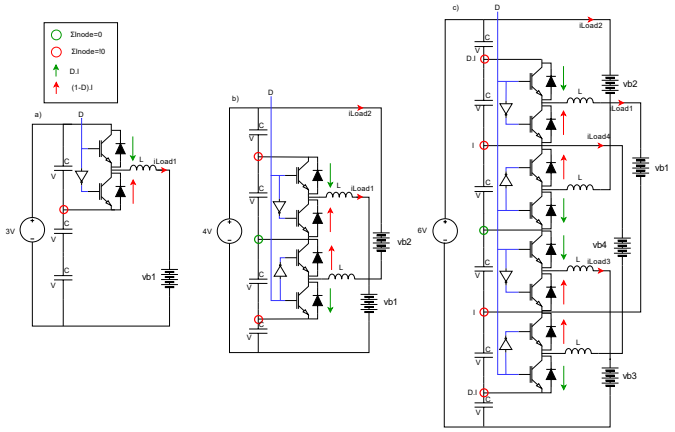

Fig. 1.Topologies for controlling battery current by regulatin terminal voltage between 2V and 3V. (a) Partial Buck converter with Capacitive voltage divider, (b) Extra cells must be added to compensate for non-zero average current at some of the capaacitive nodes, (c) Minimal converter shape with four stabilizing points and one balancing point. Adding more cellw will not reduce the number of non-stable nodes.

To address this issue, it is imperative to stabilize the four problematic nodes. The two lowermost nodes can be regulated at potentials V and 2V by means of an auxiliary battery and two switching cells (Fig. 2). These cells serve to stabilize the voltage across the capacitors which see currents *D.I* and *I* (cf. Fig. 1-c).

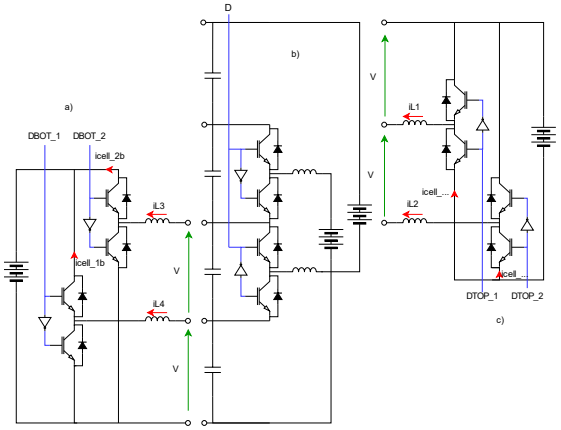

Fig. 2 Building block for modular construction. (a) Terminal bottom block (b) Generic block (c) Terminal top block

The average current in the bottom switches of the two commutations cells can be calculated as:

$$\begin{cases} < i_{cell1_b} >= D_{BOT\_1}. < i_{L4} >= \dfrac{V}{V_b}.D.I \\ < i_{cell2_b} >= D_{BOT\_2}. < i_{L3} >= \dfrac{2V}{V_b}.I \end{cases} \quad (1)$$

In this study, the voltage of the auxiliary cells was set to the same values as the inner cells: V_b. Therefore, D is equivalent for all inner commutation cells and can be expressed as:

$$D = \frac{V_b - 2V}{V} \quad (2)$$

The following equations have been developed to express the average current drawn by the auxiliary battery:

$$\begin{aligned} < i_{b_{aux2}} > &= < i_{cell1_b} > + < i_{cell2_b} > \\ &= \frac{V}{V_b}.\frac{V_b - 2V}{V}.I + \frac{2V}{V_b} \quad => \\ &< i_{b_{aux2}} > = I \end{aligned} \quad (3)$$

The result of (3) indicates that the auxiliary battery, which is employed to stabilize lower nodes, contributes an equivalent amount to that of the inner battery. The device exhibits a consistent voltage and current under these conditions, reaching its maximum capacity. Consequently, the battery does not incur an additional cost. A similar demonstration can be executed for the upper nodes, yielding a similar conclusion.

3. General Construction

The construction of the TLPVC is analogous to assembling a LEGO structure. The system is built using components derived from the three generic blocks, as illustrated in Fig. 2

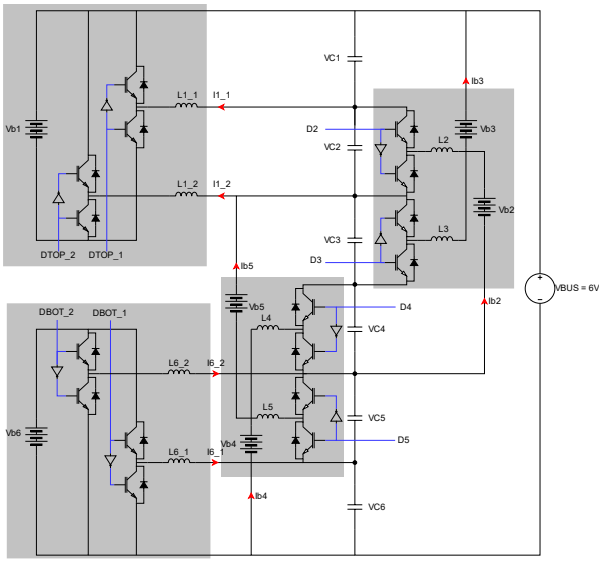

Fig. 3 An exemple of extrapolating the construction principle for an 6-battery structure with generic, top and bottom block idenfied

The system is governed by the following set of equations. First, the average voltage generated by the commutation cells (*avgV)* is considered. Second, Kirchhoff's Voltage Law is applied to the main loop, which includes capacitors C_1 to C_6 and the bus (*KVLm)*. Third, Kirchhoff's Current Law is applied to the batteries 1 and 6 (*KCLb)*. Finally, Kirchhoff's Current Law is applied to the nodes shared by adjacent capacitors C_k and C_{k+1}, for k = 1 to 5 (*KCLc*).

$$\left.\begin{aligned} D_{Top_1}V_{b_1} &= V_{C_1} \\ D_{Top_2}V_{b_1} &= V_{C_1}+V_{C_2} \\ D_2V_{C_2} &= V_{b_2} - V_{C_3} - V_{C_4} \\ D_3V_{C_3} &= V_{b_3} - V_{C_2} - V_{C_1} \\ D_4V_{C_4} &= V_{b_4} - V_{C_5} - V_{C_6} \\ D_5V_{C_5} &= V_{b_5} - V_{C_4} - V_{C_3} \\ D_{Bot_2}V_{b_6} &= V_{C_5}+V_{C_6} \\ D_{Bot_1}V_{b_6} &= V_{C_6} \end{aligned}\right\} \Rightarrow avgV \qquad 4$$

$$V_{bus} = \sum_{k=1}^{6} V_{C_k} \qquad \Rightarrow KVLm \qquad 5$$

$$\left.\begin{aligned} I_{b_1} &= D_{Top_1}I_{1_1}+D_{Top_2}I_{1_2} \\ I_{b_6} &= D_{Bot_1}I_{6_1}+D_{Bot_2}I_{6_2} \end{aligned}\right\} \Rightarrow KCLb \qquad 6$$

$$\left.\begin{aligned} I_{1_1} &= D_2I_{b_2} \\ I_{1_2} + (1-D_3)I_{b_3} &= I_{b_5} + (1-D_2)I_{b_2} \\ D_3I_{b_3} &= D_4I_{b_4} \\ I_{6_2} + (1-D_4)I_{b_4} &= I_{b_2} + (1-D_5)I_{b_5} \\ I_{6_1} &= D_5I_{b_5} \end{aligned}\right\} \Rightarrow KCLc \qquad 7$$

This modular approach facilitates system construction by combining the three types of blocks. These include a terminal block, an arbitrary number of generic blocks, and a terminal top block. Such an architecture ensures both scalability and efficiency. Indeed, the generic blocks benefit from the 'triple power effect' with a SCUI (Semiconductor Utilization Index) in [2;3], while the terminal blocks are conventional, with their SCUI lying in [1/3;1].

4. Sensitivity to Battery Parameters

In this section, the operation of the architecture depicted in Fig. 3 will be examined in the context of unbalanced sources. To that end, the following assumptions will be made:

- the full DC voltage V_{Bus} will be referred to as 6V,
- standard voltage loops (not detailed here) allow to regulate the two outputs of the auxiliary block at respectively V and 2V,
- the generic blocks are controlled by different duty cycles adjusted by standard control loops that regulate the current flowing in each battery,
- the battery open circuit voltages are the inputs of the problem to be solved; their values should represent the parameters spread of sources of identical nature and commercial reference (e.g. batteries of the same model); typical differences might be 10-20%.

This section elucidates the methodology for determining the steady-state voltage distribution across capacitors C_1 to C_6 in the presence of unbalanced battery voltages v_{b1} to v_{b6}.

The following development focuses on the average model of each commutation cell within the generic block. Based on the primary and secondary assumptions, the resulting equation can be formulated

$$v_{c1} = v_{c2} = v_{c5} = v_{c6} = \frac{V_{Bus}}{6} = V \qquad 8$$

With (8), four of six capacitor voltages are known. For the last capacitor voltages, we will focus on the two central commutation cells (associated to v_{b3} and v_{b4}). The node between those needs to see a current with zero average value to avoid v_{c3} and v_{c4} to drift. If we now focus on voltages, we can write four equations, one imposed by (8) and three equations based on Kirchhoff's Voltage Laws.

$$\begin{cases} D_3I_{b3} = D_4I_{b4} \\ v_{C3} + v_{C4} = \dfrac{V_{Bus}}{3} = 2V \\ v_{b3} = 2V + D_3v_{c3} \\ v_{b4} = 2V + D_4v_{c4} \end{cases} \qquad 9$$

Based on the system (9) we can work with equations and finally express v_{c4} and v_{c3} capacitor voltages based on the converter parameters (battery voltages and currents, V_{Bus}).

$$v_{c4} = 2V.\frac{(v_{b4}-2V)I_{b4}}{(v_{b3}-2V)I_{b3} + (v_{b4}-2V)I_{b4}} \qquad 10$$

v_{c3} is obtained with injection of (10) in the second expression of (9). With those equations, it is now possible to evaluate the impact of battery voltage variations on the partial converter when each battery current is regulated by its own current loop.

5. Simulation

This section presents preliminary simulation used to validate the equations describing the converter's steady-state behavior. To remain consistent with the previously stated assumptions, the auxiliary commutation cells are replaced by independent voltage sources V and 2V. These sources emulate voltage regulation in this initial simulation.

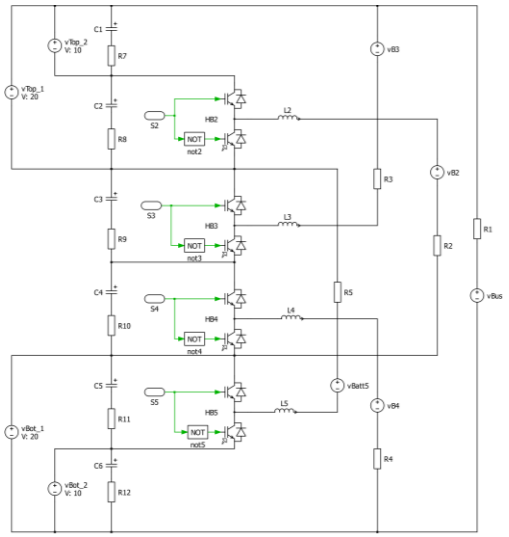

Fig. 4 PLECS model of the TLPCV 6-battery converter with auxiliary modules substituted with voltage source

Table 1 TLPVC parameters

Parameter	Value
L	208µH
C	125µF
$R_{2\ldots5}$	10mΩ
$R_{1,\ 7\ldots12}$	100µΩ
V_{Bus}	60V
V_{B2}	27.5V
V_{B3}	24V
V_{B4}	25.2V
V_{B5}	23V
fsw	20kHz

5.1. *Current control loop*

The control system consists of four independent current loops, each implemented using a PI regulator. To illustrate this, consider the voltage mesh associated with v_{b4}, as shown in Fig. 4.

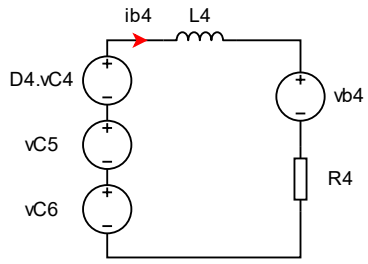

Fig. 5 Equivalent circuit of battery 4 voltage mesh

After isolating the expression for i_{b4} and applying the Laplace transform, we obtain:

$$i_{b4}(s) = \frac{D_4 \times v_{c4} + v_{C5} + v_{c6} - v_{b4}}{L_4 \times s + R_4} \qquad 11$$

Based on (11), the following synopsis of the current control loop can be created:

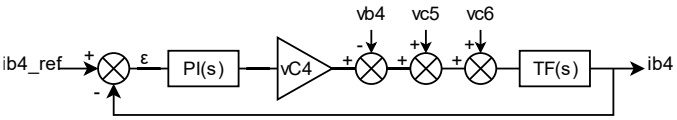

Fig. 6 Full current loop synopsis for v_{b4} arm of the TPLCV

In this study, v_{b4}, v_{C5} and v_{C6} are often neglected for two main reasons. First, although these quantities contribute to the static error, this error is ultimately eliminated by the integral action of the PI regulator. Second, their measurement would require additional sensors, increasing the system cost and contradicting the converter's design philosophy.

The transfer function considered is as follows:

$$TF(s) = \frac{I(s)}{D} = \frac{1}{L_4 \times s + R_4} \approx \frac{1}{L_4 \times s} \qquad 12$$

Due to this low value, R_4 is neglected. The final expression of (12) is used to determine the coefficient values of the PI corrector *Kd* and *Ki* (parallel form).

5.2. *First result*

The selection of the four reference current values was based on a specific set of criteria. The nominal current was defined as 2A, and the nominal battery voltage was set at 25V. A deviation of the battery voltage from this 25V reference leads to an increase in the charging current, and vice versa. Table 1 lists the different current setpoints.

Table 2 Charging current values for each battery

Current name	**Value**
I_{b2_ref}	1A
I_{b3_ref}	2A
I_{b4_ref}	1.7A
I_{b5_ref}	3A

The battery currents and the capacitor voltages are presented in Fig. 7. As expected, v_{C1} = v_{C2} = v_{C5} = v_{C6} = 10V (voltage sources). Among the 60V present at the input bus, a total of 20V is allocated for distribution between voltage v_{C3} and v_{C4}. This phenomenon is illustrated in Fig. 7, where the voltages exhibit a transient variation before oscillating between steady-state values of 15V and 5V, respectively. As a result, the associated currents also oscillate, since they depend directly on these voltages. Such behavior is undesirable and indicates that regulating at least one of the capacitor voltages is necessary.

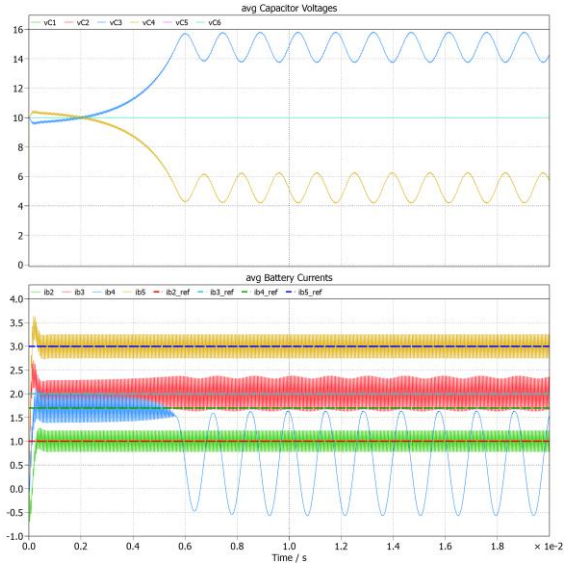

Fig. 7 First simulaton result of the TLPVC with current loop regulation

5.3. *Voltage control loop*

As demonstrated in the preceding section, the determination of converter operating points is contingent upon the parameters that define the converter's functionality. These parameters include the battery voltages, the bus voltage, and the battery current setpoint. The decision was made that the voltage v_{C4} would be regulated by the control loop, thereby imposing v_{C3}.

According to the stipulated parameters of the simulation, the corresponding v_{C4} value is determined to be 10.4988V. This value is defined as the reference value for the control loop.

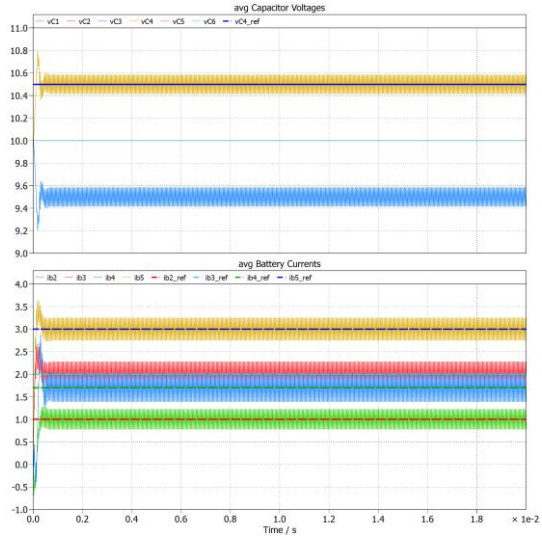

Fig. 8. Simulation result of the converter with all current regulated and vC4 regulated

Voltage regulation has been demonstrated to stabilize the capacitors' voltages. It is evident that their values align with the established expectations (i.e. v_{C4} = 10.4988V and v_{C3} = 9.5012V). This stability is further evidenced by the current measurements in each battery, which are consistently with the established parameters.

5.4. Simulation perspectives

Next, we will implement voltage control loops for the auxiliary switchgear. Under the current assumptions, the terminal capacitor-pair voltages are fixed at V and 2V. Alternatively, one could regulate the auxiliary inductor currents to match the unstabilized node currents.

6. Experimentation

To minimize the carbon footprint of this work, an experimental setup capable of supporting multiple configurations was developed, building on an existing platform previously used for a 3-phase, 5-level-per-phase flying capacitor inverter and a 12-phase interleaved converter with InterCell Transformer. For this third application, only the power PCB was modified. The updated configuration features a top terminal block, a bottom terminal block, and four generic blocks. By selectively shorting certain blocks, the setup can accommodate 6-, 8-, 10-, and 12-battery configurations

The batteries used in the setup are 39Ah, 3.2V $LiFePO_4$ cells. All control operations are carried out using an RT-BOX. For safety purposes, each battery is individually monitored, and a shutdown signal is triggered if any cell voltage exceeds its upper or lower threshold.

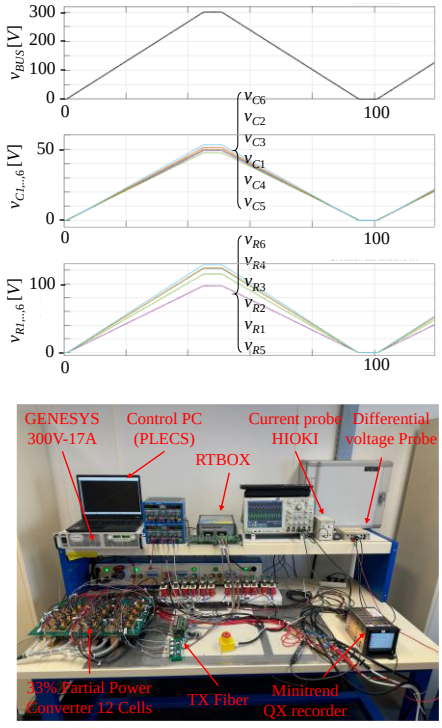

Fig. 9Experimental setup (inductors and TLPV Converter)

7. Conclusion

This paper introduced a converter topology enabling controlled charging and discharging of a battery pack. A key characteristic of this architecture is its ability to process power levels typically two to three times higher than what the employed semiconductors are conventionally rated for. This approach holds promise for reducing costs and improving overall efficiency, although these benefits must be confirmed through experimental validation.

The proposed converter is suitable for both high- and low-power or voltage applications, and it opens the door to implementations using a wide range of semiconductor technologies and switching frequencies. Regardless of the specific choices, the high SCUI is expected to provide advantages across all scenarios.

8. References

[1] R. M. Button, "An advanced photovoltaic array regulator module," in *IECEC 96. Proceedings of the 31st Intersociety Energy Conversion Engineering Conference*, Aug. 1996, pp. 519–524 vol.1. doi: 10.1109/IECEC.1996.552937.

[2] Y. Cao, M. Ngo, N. Yan, D. Dong, R. Burgos, and A. Ismail, "Design and Implementation of an 18-kW 500-kHz 98.8% Efficiency High-Density Battery Charger With Partial Power Processing," *IEEE J. Emerg. Sel. Top. Power Electron.*, vol. 10, no. 6, pp. 7963–7975, Dec. 2022, doi: 10.1109/JESTPE.2021.3108717.

[3] P. Granello, T. B. Soeiro, N. H. van der Blij, and P. Bauer, "Revisiting the Partial Power Processing Concept: Case Study of a 5-kW 99.11% Efficient Flyback Converter-Based Battery Charger," *IEEE Trans. Transp. Electrification*, vol. 8, no. 3, pp. 3934–3945, Sep. 2022, doi: 10.1109/TTE.2022.3170286.

[4] V. M. Iyer, S. Gulur, S. Bhattacharya, and R. Ramabhadran, "A Partial Power Converter Interface for Battery Energy Storage Integration with a DC Microgrid," in *2019 IEEE Energy Conversion Congress and Exposition (ECCE)*, Sep. 2019, pp. 5783–5790. doi: 10.1109/ECCE.2019.8912590.

[5] M. C. Mira, Z. Zhang, K. L. Jørgensen, and M. A. E. Andersen, "Fractional Charging Converter With High Efficiency and Low Cost for Electrochemical Energy Storage Devices," *IEEE Trans. Ind. Appl.*, vol. 55, no. 6, pp. 7461–7470, Nov. 2019, doi: 10.1109/TIA.2019.2921295.

[6] J. Qi and D. Dah-Chuan Lu, "A flyback converter based partial power processing structure for BESS with voltage/current regulation and battery balancing functionalities," in *2017 IEEE International Telecommunications Energy Conference (INTELEC)*, Oct. 2017, pp. 381–386. doi: 10.1109/INTLEC.2017.8214166.

[7] O. Gsous, R. Rizk, A. Barbón, and R. Georgious, "Review of DC-DC Partial Power Converter Configurations and Topologies," *Energies*, vol. 17, no. 6, Art. no. 6, Jan. 2024, doi: 10.3390/en17061496.

[8] J. Anzola *et al.*, "Review of Architectures Based on Partial Power Processing for DC-DC Applications," *IEEE Access*, vol. 8, pp. 103405–103418, 2020, doi: 10.1109/ACCESS.2020.2999062.

[9] K. Zheng, W. Zhang, X. Wu, and L. Jing, "Optimal Control Method and Design for Modular Battery Energy Storage System Based on Partial Power Conversion," *IEEE Access*, vol. 9, pp. 133376–133386, 2021, doi: 10.1109/ACCESS.2021.3115944.

[10] R. V. Jyothsna, A. A. Dar, S. Kadam, and V. M. Iyer, "Non-Isolated Partial Power Processing Converter for Battery Energy Storage Systems," in *2024 IEEE International Communications Energy Conference (INTELEC)*, Aug. 2024, pp. 1–6. doi: 10.1109/INTELEC60315.2024.10679021.

[11] F. Xue, R. Yu, and A. Huang, "Fractional converter for high efficiency high power battery energy storage system," in *2017 IEEE Energy Conversion Congress and Exposition (ECCE)*, Oct. 2017, pp. 5144–5150. doi: 10.1109/ECCE.2017.8096866.

[12] Z. Xia and J. A. A. Qahouq, "Lithium-Ion Battery Ageing Behavior Pattern Characterization and State-of-Health Estimation Using Data-Driven Method," *IEEE Access*, vol. 9, pp. 98287–98304, 2021, doi: 10.1109/ACCESS.2021.3092743.